A role of histone H3 lysine 4 methyltransferase components in endosomal trafficking

Zhuojin Xu,[1,2] Qiang Gong,[1,2] Bin Xia,[1,3] Benjamin Groves,[1,2] Marc Zimmermann,[1] Chris Mugler,[1] Dezhi Mu,[3] Brian Matsumoto,[2] Matthew Seaman,[4,5] and Dzwokai Ma[1,2]

[1]Department of Molecular, Cellular, and Developmental Biology and [2]Neuroscience Research Institute, University of California, Santa Barbara, Santa Barbara, CA 93106
[3]Department of Pediatrics, West China Second Hospital, Sichuan University, Chengdu, Sichuan Province, China 610041
[4]Cambridge Institute for Medical Research and [5]Department of Clinical Biochemistry, University of Cambridge, Cambridge, England CB2 0XY, UK

Histone lysine methyltransferase complexes are essential for chromatin organization and gene regulation. Whether any of this machinery functions in membrane traffic is unknown. In this study, we report that mammal Dpy-30 (mDpy-30), a subunit of several histone H3 lysine 4 (H3K4) methyltransferase (H3K4MT) complexes, resides in the nucleus and at the trans-Golgi network (TGN). The TGN targeting of mDpy-30 is mediated by BIG1, a TGN-localized guanine nucleotide exchange factor for adenosine diphosphate ribosylation factor GTPases. Altering mDpy-30 levels changes the distribution of cation-independent mannose 6-phosphate receptor (CIMPR) without affecting that of TGN46 or transferrin receptor. Our experiments also indicate that mDpy-30 functions in the endosome to TGN transport of CIMPR and that its knockdown results in the enrichment of internalized CIMPR and recycling endosomes near cell protrusions. Much like mDpy-30 depletion, the knockdown of Ash2L or RbBP5, two other H3K4MT subunits, leads to a similar redistribution of CIMPR. Collectively, these results suggest that mDpy-30 and probably H3K4MT play a role in the endosomal transport of specific cargo proteins.

Introduction

Covalent histone modifications regulate chromatin structure and function. Methylation of lysine residues within histones H3 and H4 by histone lysine methyltransferase complexes is one such modification. Depending on the site of the modified lysine residue and the extent of methylation (mono-, di-, or trimethylated), these modifications can lead to either activation or repression of transcription (Ng et al., 2009). Emerging evidence indicates an intimate link between abnormal histone methylation and human disease. Although histone lysine methyltransferase complexes primarily reside in the nucleus and target histones, their presence in the cytosol has been suggested (Su et al., 2005), and several nonhistone substrates have been identified (Huang and Berger, 2008). Based on our knowledge, whether a histone lysine methyltransferase complex or its subunits reside or function in the intracellular vesicular transport pathway is currently unknown. In this regard, an organellar proteomic study has detected arginine dimethylation in several Golgi proteins and revealed two putative Golgi-associated methyltransferases (Wu et al., 2004).

In mammals, at least five different SET1 family methyltransferase complexes target histone H3 lysine 4 (H3K4; Ruthenburg et al., 2007; Shilatifard, 2008). Although these complexes contain distinct catalytic subunits, they share common components, including Ash2L, RbBP5, WDR5, and mammal Dpy-30 (mDpy-30). Ash2L, RbBP5, and WDR5 form a stable core complex that confers substrate specificity and controls catalytic activity (Dou et al., 2006; Steward et al., 2006). Dpy-30 was originally identified as an essential component of *Caenorhabditis elegans* dosage compensation machinery (Hsu et al., 1995). However, Dpy-30 mutant males also exhibit growth and development defects, indicating a general function of this protein. Subsequent studies have demonstrated that the yeast and mammalian orthologues of Dpy-30, Sdc1 (Miller et al., 2001; Roguev et al., 2001) and mDpy-30 (Hughes et al., 2004; Cho et al., 2007), respectively,

Z. Xu, Q. Gong, and B. Xia contributed equally to this paper.

Correspondence to Dzwokai Ma: ma@lifesci.ucsb.edu

Abbreviations used in this paper: CIMPR, cation-independent mannose 6-phosphate receptor; Flp, flippase recombination enzyme; mDpy-30, mammal Dpy-30; PM, plasma membrane; TfnR, transferrin receptor.

The Rockefeller University Press $30.00
J. Cell Biol. Vol. 186 No. 3 343–353
www.jcb.org/cgi/doi/10.1083/jcb.200902146

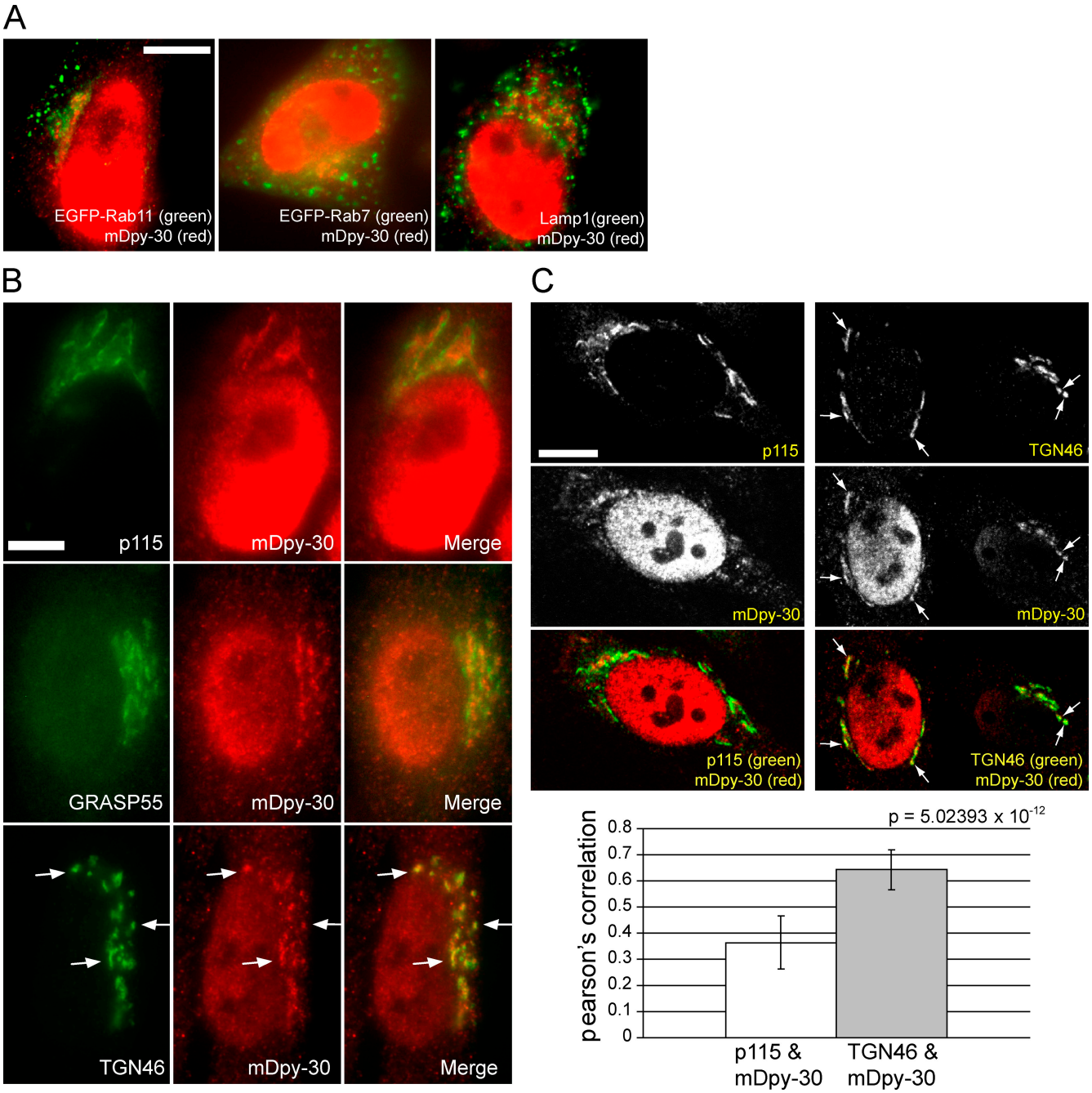

Figure 1. **Imaging analyses of perinuclear mDpy-30 in HeLa cells.** (A–C) Cells were fixed in 3% formaldehyde, permeabilized with 0.1% saponin, immunostained, and visualized using conventional (A and B) or confocal (C) microscopy. Arrows indicate sites of colocalization. (A) Colocalization analysis of mDpy-30 and recycling endosomes (EGFP-Rab11), late endosomes (EGFP-Rab7), and lysosomes (Lamp1). (B) Colocalization analysis of mDpy-30 and the cis-Golgi network/cis-Golgi (p115), medial-Golgi (GRASP55), or TGN (TGN46) marker. (C) Colocalization analysis of mDpy-30 and p115 or TGN46. A representative image from single z section is shown (the full z stack for both are available in the JCB DataViewer; http://jcb-dataviewer.rupress.org/jcb/browse/1505/2600). Pearson's correlations were calculated from each image in the z stack of confocal microscopy images of the perinuclear regions (defined by p115 or TGN46) using the colocalization analysis from Image-Pro Plus 3.6 software (Media Cybernetics; Student's *t* test, $P = 5.02393 \times 10^{-12}$; $n = 14$). Error bars indicate the standard deviation of the values obtained from individual cells. Bars, 10 µm.

are common subunits of several H3K4 methyltransferase (H3K4MT) complexes and that deletion of Sdc1 from yeast leads to a greatly reduced level of H3K4 trimethylation (Schneider et al., 2005). Despite being a conserved H3K4MT subunit, the molecular function of mDpy-30 remains unknown. We originally isolated mDpy-30 from a rat brain cDNA library as a potential binding partner of a potassium channel in a yeast two-hybrid screen. Although we have not been able to confirm the interaction between mDpy-30 and the channel protein, we found that mDpy-30 localized to the Golgi apparatus and proceeded to examine the role of mDpy-30 in vesicular traffic.

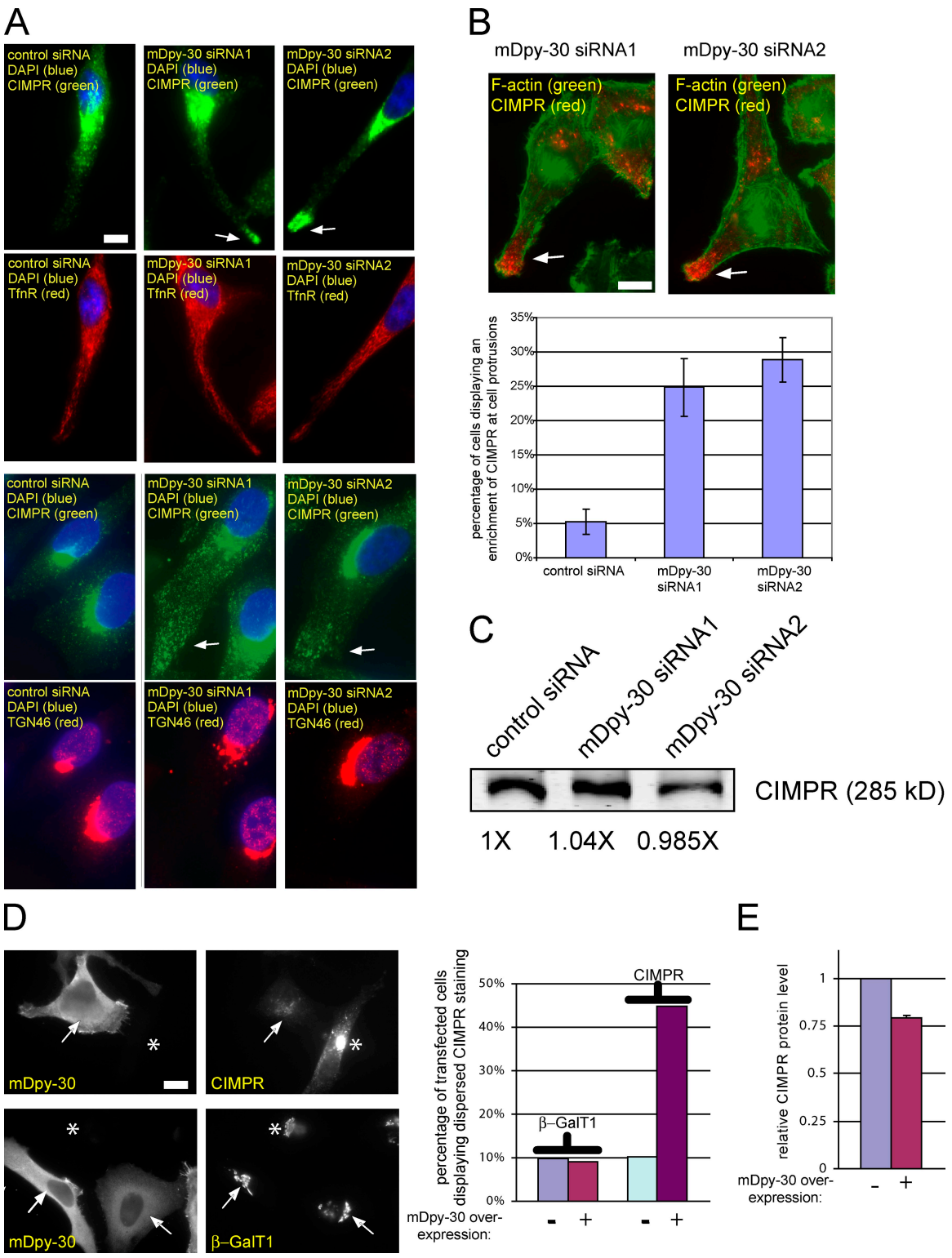

Figure 2. **Subcellular distribution analyses of CIMPR, TGN46, and TfnR in HeLa cells depleted of or overexpressing mDpy-30.** All siRNAs were used at a concentration of 20 nM, and transfected cells were analyzed 48 h after transfection. Unless noted otherwise, the values shown in all bar graphs and Western blots are the mean results obtained from at least three independent experiments. For imaging analyses, >500 cells were counted in each experiment. (A) Subcellular distributions of CIMPR, TGN46, or TfnR in HeLa cells treated with control nontargeting or mDpy-30 siRNAs. Cells were processed as described in Fig. 1. Arrows indicate cell protrusions. (B) Enrichment of CIMPR near cell protrusions (indicated by arrows) was confirmed by phalloidin F-actin costaining, and the fraction of cells displaying enriched CIMPR near protrusions was scored. (C) Western blot analysis of the CIMPR protein level after the knockdown of mDpy-30. The numbers represent the mean value of six independent experiments. (D) The effect of mDpy-30 overexpression on the localization of CIMPR or β-GalT1 (compare asterisks with arrows). Only those cells exhibiting a high level of exogenous mDpy-30 were counted. The experiment was repeated once, and the mean value is shown. (E) The protein level of CIMPR in cells overexpressing mDpy-30. (B and E) Error bars indicate the standard deviation of the values obtained from independent experiments. Bars, 10 μm.

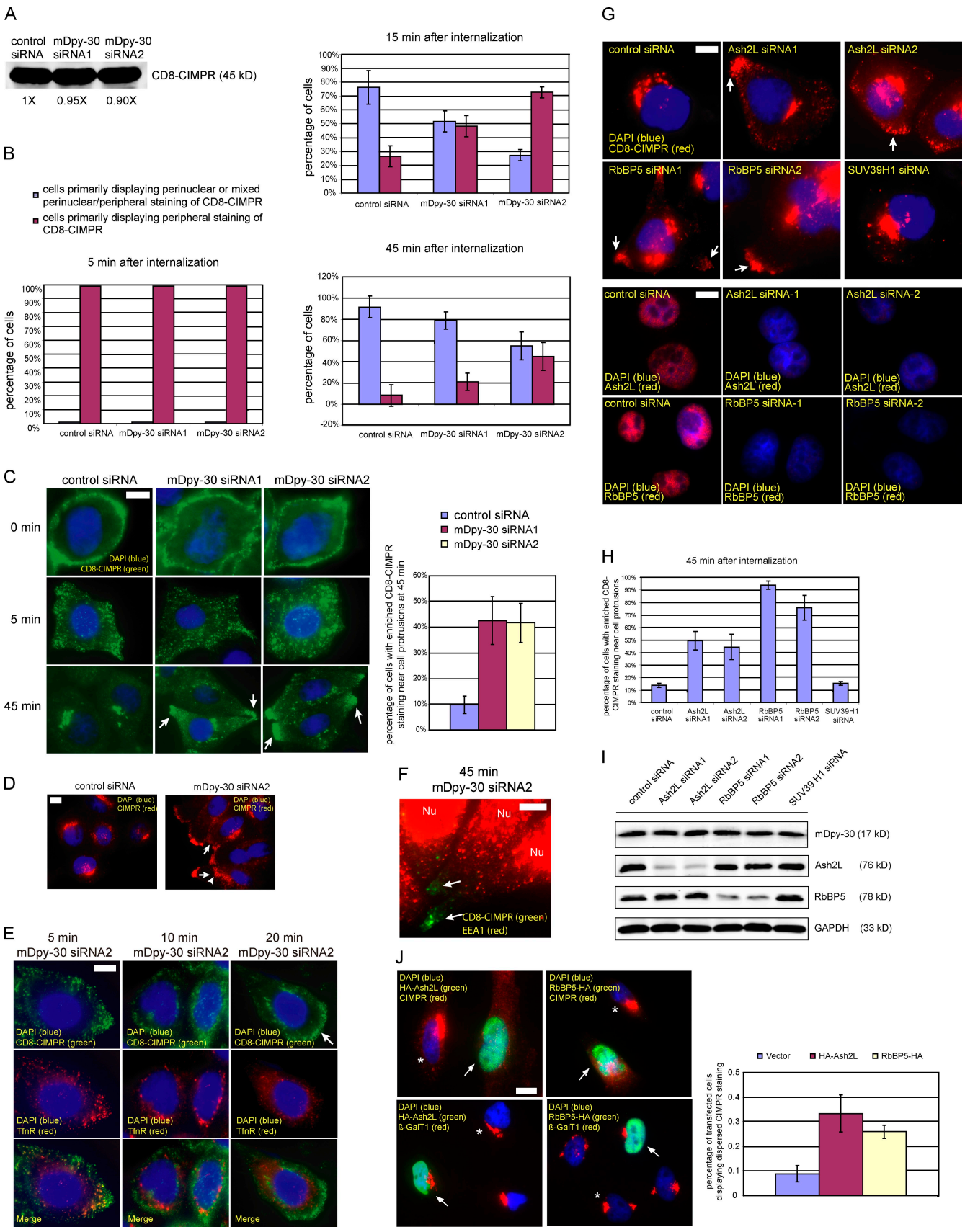

Figure 3. **The role of mDpy-30 in the endosome to TGN transport of CIMPR in HeLa cells.** Transfection and staining were performed as described in Figs. 2 and 1, respectively, except in G and J where 0.1% Triton X-100 was used to assure even permeabilization of the nuclear membrane among cells. The values shown in all bar graphs and Western blots are the mean results obtained from at least three independent experiments. In the case of imaging analyses, >500 cells were counted in each experiment. Except in J, arrows and the arrowhead indicate cell protrusions. (A) The impact of mDpy-30 knockdown on

Results and discussion

TGN localization of mDpy-30

Immunofluorescence study in multiple cell types revealed that mDpy-30 displayed an unanticipated dual localization, both nuclear and cytoplasmic (see Fig. S1 for antibody characterization), the latter of which was enriched at a perinuclear site (Fig. S1 E). The following observations suggest that the dual localization is an intrinsic property of mDpy-30. First, an HA-tagged mDpy-30 exhibited a similar distribution when stably expressed in CV-1 cells (Fig. S1 G). Second, live cell imaging indicated that a pool of mDpy-30–monomeric RFP (monomeric RFP fused to the C terminus of mDpy-30) resided in a perinuclear region in addition to the nucleus (Fig. S1 H). To define the identity of perinuclear mDpy-30 staining, we conducted a comparison between perinuclear mDpy-30 and subcellular markers known to reside in compartments near the nucleus (Fig. 1 A). We found little or no colocalization between mDpy-30 and recycling endosomes (labeled by an EGFP fusion of Rab11; Ullrich et al., 1996), late endosomes (EGFP fusion of Rab7; Meresse et al., 1995), and lysosomes (Lamp1; Chen et al., 1985). When compared with Golgi markers (Fig. 1 B), mDpy-30 displayed little colocalization with p115, a cis-Golgi network/cis-Golgi marker (Nelson et al., 1998), and GRASP55, a medial-Golgi marker (Shorter et al., 1999). However, mDpy-30 staining was in close proximity to and partially overlapped with that of TGN46, a TGN marker (Ponnambalam et al., 1996). Similar results were obtained using confocal microscopy (Fig. 1 C and JCB DataViewer; http://jcb-dataviewer.rupress.org/jcb/browse/1505/2600); Pearson's correlation analysis indicated that there was a significantly higher correlation between the TGN46 and mDpy-30 staining than that of p115 and mDpy-30. Collectively, our data suggest that a pool of mDpy-30 is present at the TGN.

Altered subcellular distribution of cation-independent mannose 6-phosphate receptor (CIMPR) but not TGN46 or transferrin receptor (TfnR) in cells depleted of or overexpressing mDpy-30

As an H3K4MT subunit, the TGN localization of mDpy-30 was unexpected and implied a potential role of this protein in membrane traffic. To test whether mDpy-30 was involved in TGN trafficking, we investigated the impact of depleting or overexpressing mDpy-30 on the subcellular distributions of three cargo proteins that cycle among the TGN, plasma membrane (PM), and endosomes, including TGN46 (which traffics from the TGN to the PM to early/recycling endosomes and back to the TGN [Ghosh et al., 1998; Mallard et al., 2002; Ganley et al., 2008]), CIMPR (which moves from the TGN to early/recycling endosomes to late endosomes and back to the TGN or from the TGN to the PM to early/recycling endosomes to late endosomes to the TGN [Ghosh et al., 2003]), and TfnR (which cycles between the PM and early/recycling endosomes [Maxfield and McGraw, 2004]).

We first compared the subcellular distributions of TGN46, CIMPR, and TfnR in HeLa cells transfected with a nontargeting control or mDpy-30 siRNA (see Fig. S2 for siRNA characterization). Although both control and mDpy-30 knockdown cells expressed a similar level of CIMPR (Fig. 2 C), depletion of mDpy-30 resulted in a five- to sixfold increase in the fraction of cells displaying an enrichment of CIMPR near cell protrusions (Fig. 2, A and B). In contrast, neither TGN46 nor TfnR became concentrated in these compartments. The distribution of CIMPR was also more sensitive to mDpy-30 overexpression (i.e., a reduced perinuclear and an increased dispersed staining compared with control cells) than those of β-GalT1 (Fig. 2 D) and TGN46 (not depicted). Moreover, the overexpression of mDpy-30 caused a 25% reduction of CIMPR protein level (Fig. 2 E), possibly by promoting its lysosomal degradation.

Function of mDpy-30 in CIMPR endosomal transport

We next investigated the effect of depleting mDpy-30 on CIMPR endosomal transport in a HeLa cell line stably expressing a CD8 fusion of CIMPR. A previous study has shown that the trafficking properties of this fusion are identical to those of endogenous CIMPR (Seaman, 2004). Western blot analysis indicated that mDpy-30 knockdown had no significant influence on the level of CD8-CIMPR (Fig. 3 A).

We labeled surface CD8-CIMPR using an anti-CD8 antibody and followed the endosomal transport at different time points after internalization (Fig. 3, B and C). At 5 min after internalization, CD8-CIMPR was primarily found in peripheral vesicles (presumably early endosomes) in virtually all control and mDpy-30–depleted cells, suggesting that mDpy-30 depletion had no substantial impact on the internalization of CD8-CIMPR.

the protein level of CD8-CIMPR fusion expressed in a HeLa stable line. (B and C) The effect of mDpy-30 depletion on the endosomal transport of CD8-CIMPR monitored at different time points after internalization as described in Materials and methods. Cells were analyzed by eye using the following criteria. In B, cells were scored as perinuclear or mixed perinuclear/peripheral if internalized CD8-CIMPR could be detected as a distinct perinuclear structure in close proximity to TGN46. However, cells lacking such structure were scored as peripheral. In C, cells were scored based on whether internalized CD8-CIMPR became enriched near cell protrusions as described in Fig. 2 B. (D) The influence of knocking down mDpy-30 on the endosomal transport of endogenous CIMPR in HeLa cells was assessed after adding anti-CIMPR antibody to the culture medium for 1 h at 37°C. (E) The comparison of the endosomal transport of CD8-CIMPR and TfnR in mDpy-30–depleted HeLa stable cells. Surface TfnR and CD8-CIMPR were labeled with biotinylated transferrin and the anti-CD8 antibody, respectively, and their endosomal transport was examined at 5, 10, and 20 min after internalization. (F) EEA1 staining was absent at the CD8-CIMPR–enriched cell protrusions. Nu, nucleus. (G and H) The influence of depleting Ash2L or RbBP5 (two H3K4MT components) and SUV39H1 (a component of H3K9MT) on the targeting of internalized CD8-CIMPR to cell protrusions. The effectiveness of Ash2L and RbBP5 siRNAs was examined using immunofluorescence and Western blot (see I) analyses. Cells were scored according to the criteria described in Fig. 2 B, and the result is shown in the bar graph. (I) The impact of knocking down Ash2L or RbBP5 on the protein level of mDpy-30. The level of GAPDH (glyceraldehyde-3-phosphate dehydrogenase) was used as a loading control. (J) The effects of Ash2L or RbBP5 overexpression on the localization of CIMPR or β-GalT1 (compare asterisks with arrows). (B, C, H, and J) Error bars indicate the standard deviation of the values obtained from independent experiments. Bars, 10 μm.

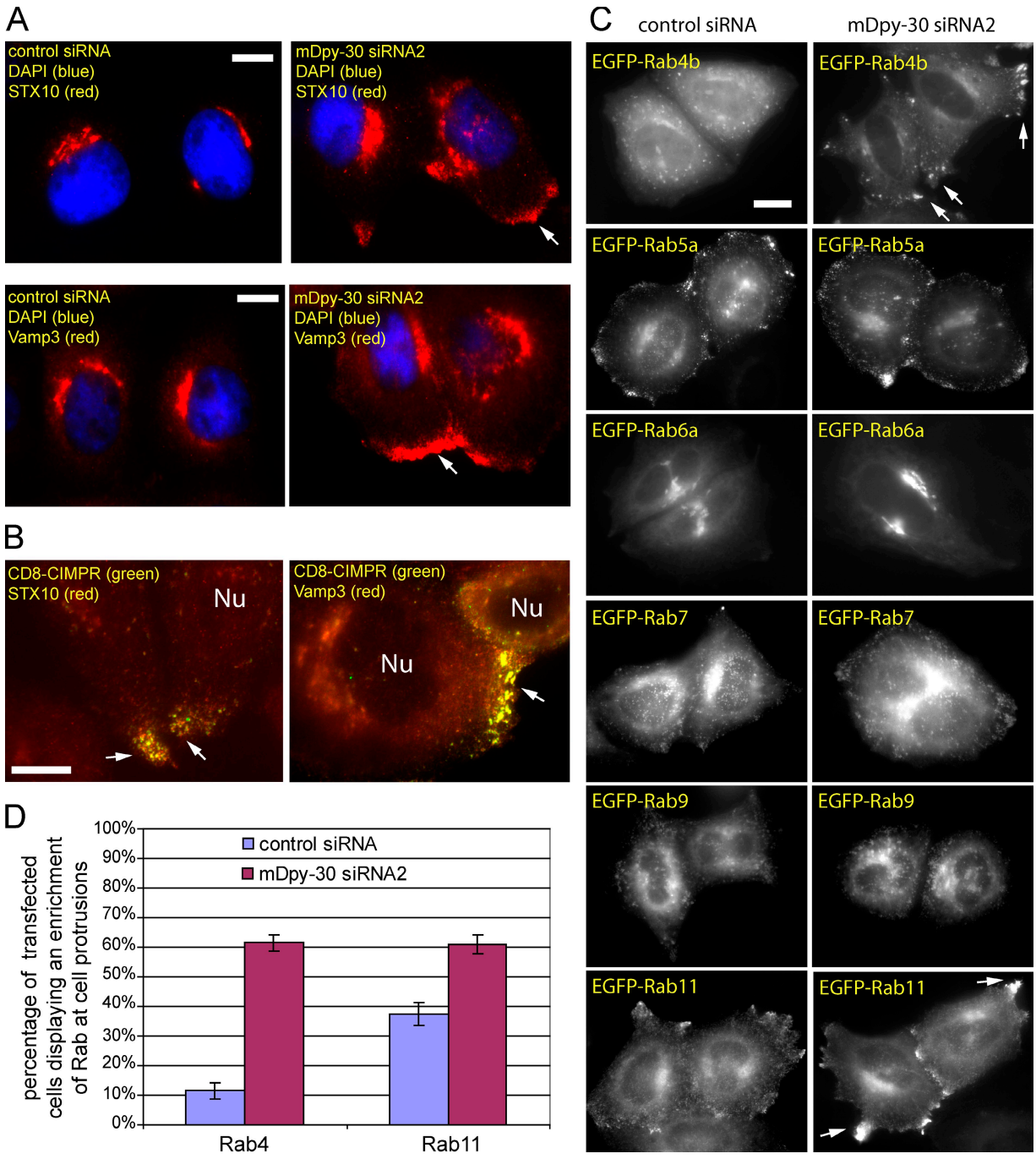

Figure 4. **Characterization of the CIMPR-enriched compartment at cell protrusions.** Transfection and staining were conducted as described in Figs. 2 and 1, respectively. Arrows indicate cell protrusions. (A) The localization of STX10 and VAMP3 after mDpy-30 knockdown. (B) Colocalization analysis of internalized CD8-CIMPR and STX10 or VAMP3 near cell protrusions. Internalization was performed as described in Fig. 3. Nu, nucleus. (C and D) The influence of mDpy-30 knockdown on the localization of various endosomal Rab proteins in HeLa–CD8-CIMPR stable cells. EGFP fusions of Rab proteins were transfected into cells pretreated with a nontargeting control or mDpy-30 siRNA2, and transfected cells were scored according to the criteria described in Fig. 2 B. The numbers in the bar graph represent the mean result from five independent experiments ($n > 500$ in each experiment). Error bars indicate the standard deviation of the values obtained from independent experiments. Similar results were obtained with mDpy-30 siRNA1, albeit with less effect (not depicted). Bars, 10 µm.

At 15 min after internalization, a pool of CD8-CIMPR had reached a perinuclear site in ~75% of the control cells; this perinuclear compartment became the most prominently stained structure in the majority of cells. However, the fraction of cells displaying perinuclear localization of CD8-CIMPR was reduced in mDpy-30 knockdown cells (52% for siRNA1 and 27% for siRNA2). Even in those cells exhibiting a perinuclear CD8-CIMPR staining, a large fraction of fusion proteins remained in peripheral endosomes throughout the cytosol (Fig. 3 C). The difference in the perinuclear targeting of CD8-CIMPR persisted after 45 min of internalization. Accompanying this decreased efficiency in targeting internalized CD8-CIMPR to the perinuclear

region, there was a time-dependent enrichment (a fourfold increase for siRNA1 or -2) of fusion proteins at a compartment near the protrusions of mDpy-30–depleted cells (Fig. 3, B and C). To confirm that mDpy-30 knockdown exerted a similar effect on endogenous CIMPR, we added the anti-CIMPR antibody to the culture medium of HeLa cells for 1 h at 37°C. The antibody labeling and internalization steps were combined and lengthened to improve the signal strength of internalized endogenous CIMPR (Fig. 3 D). As with CD8-CIMPR, a fraction of CIMPR was found near protrusions in mDpy-30–depleted cells. Because the endosomal transport of a CD8-furin fusion was altered by mDpy-30 siRNA in a similar way (unpublished data), the effect of mDpy-30 on trafficking was not specific to CIMPR.

The observation that the level of CD8-CIMPR at the protrusions of mDpy-30 knockdown cells increased within 45 min of internalization implied that mDpy-30 functions at a late endosomal transport step. To test this, we simultaneously compared the endosomal transport of TfnR (via biotinylated transferrin) and CD8-CIMPR. As shown in Fig. 3 E, at 5 min after internalization, CD8-CIMPR and TfnR colocalized at an early endosomal compartment in both control (not depicted) and mDpy-30–depleted cells. At 10 or 20 min after internalization, TfnR entered tubular recycling endosomes, but there was little colocalization with CD8-CIMPR, indicating that these proteins had been sorted into different pathways after their transit through the early endosomes. This was in accordance with a lack of EEA1 (a marker of early endosomes) staining in the protrusion regions where internalized CD8-CIMPR became enriched (Fig. 3 F).

Collectively, our data suggest that mDpy-30 regulates the late endosomal trafficking of a subset of cargo proteins such as CIMPR and furin. Given the TGN localization of mDpy-30 as well as the inefficient return of internalized CD8-CIMPR to a perinuclear site, mDpy-30 is probably involved in the endosome to TGN transport of CIMPR. In the absence of mDpy-30, a pool of CIMPR is redirected to endosomes near cell protrusions. However, we cannot exclude a role of mDpy-30 in the transport between endosomes or from the TGN to endosomes. Moreover, because mDpy-30 knockdown also reduced the H3K4 trimethylation (Fig. S2 E), our data do not allow us to distinguish whether mDpy-30 modulates CIMPR trafficking via transcription or posttranscriptional effects or both.

A role of the H3K4MT complex or complexes in the endosomal transport of CIMPR

To explore H3K4MT involvement in trafficking, we examined the endosomal transport of CD8-CIMPR after knocking down either Ash2L or RbBP5, two other common H3K4MT subunits (Fig. 3, G and H). Indeed, cells transfected with either of the two siRNAs against Ash2L or RbBP5 accumulated internalized CD8-CIMPR near cell protrusions. The effect of Ash2L or RbBP5 siRNAs on CIMPR was not caused by their impact on the level of mDpy-30 protein (Fig. 3 I). In contrast, treatment of cells with an siRNA against SUV39H1, a component of the H3K9MT complex (Rea et al., 2000), exerted little effect. Moreover, similar to mDpy-30 overexpression, overexpression of either Ash2L or RbBP5 increased the fraction of cells displaying a dispersed CIMPR distribution without changing that of β-GalT1 (Fig. 3 J). These results indicate a link between H3K4MT and the endosomal transport of CIMPR.

Characterization of the CIMPR-positive peripheral compartment in mDpy-30 knockdown cells

Considering that the STX10–STX16–Vti1A–VAMP3 SNARE complex mediates the endosome to TGN transport of CIMPR (Ganley et al., 2008), we asked whether CIMPR colocalized with STX10 and VAMP3 at cell protrusions. Compared with control cells, after mDpy-30 knockdown, a pool of STX10 and VAMP3 also became enriched near cell protrusions (Fig. 4 A), where they exhibited a partial colocalization with internalized CD8-CIMPR (Fig. 4 B). However, VAMP4 and VAMP8, two other SNARE proteins along the TGN–PM–endosome loop (Cocucci et al., 2008; Kanwar et al., 2008), displayed little or only modest enrichment and little to no colocalization with CD8-CIMPR within this region (unpublished data).

To better define the CIMPR-positive compartment near cell protrusions, we investigated the distributions of Rab GTPase proteins in control and mDpy-30 knockdown cells. Each Rab protein has a compartment-specific localization and plays an essential role in defining the compartmental function in trafficking (Cai et al., 2007; Markgraf et al., 2007; Nielsen et al., 2008). For example, Rab4, -5, and -11 all reside in early endosomal compartments with distinct functions. Rab5 modulates endocytosis, and Rab4 and -11 control the endosomal recycling from early and recycling endosomes, respectively. However, Rab7 and -9 primarily function during the late endosomal trafficking, and Rab6 is thought to regulate endosome to TGN transport. As indicated in Fig. 4 (C and D), knockdown of mDpy-30 induced enrichment of Rab11 and, to an even higher extent, Rab4 at cell protrusions without significantly affecting the distributions of Rab5, -6, -7, and -9. This observation implies that the depletion of mDpy-30 causes a subpopulation of recycling endosomes to be enriched at cell protrusions.

BIG1-mediated recruitment of mDpy-30 to the TGN

To gain mechanistic insight into how mDpy-30 modulates endosomal trafficking, we set out to identify proteins interacting with mDpy-30. We generated CV-1 cells stably expressing a GFP fusion of mDpy-30 and used an anti-GFP antibody covalently linked to magnetic microbeads to immunoprecipitate mDpy-30–EGFP and its associated proteins. Tandem mass spectrometry analysis of the immunoprecipitate revealed several known mDpy-30–interacting partners, including Ash2L and WDR5 (two H3K4MT components), as well as a novel interacting partner, BIG1 (a TGN-localized ADP ribosylation factor guanine nucleotide exchange factor; Fig. 5 A; Morinaga et al., 1997). We confirmed the mDpy-30–BIG1 interaction using coimmunoprecipitation between mDpy-30 and a HA-tagged BIG1 (Fig. 5 B) as well as between endogenous mDpy-30 and BIG1 (Fig. 5 C). Furthermore, mDpy-30 and BIG1 colocalized

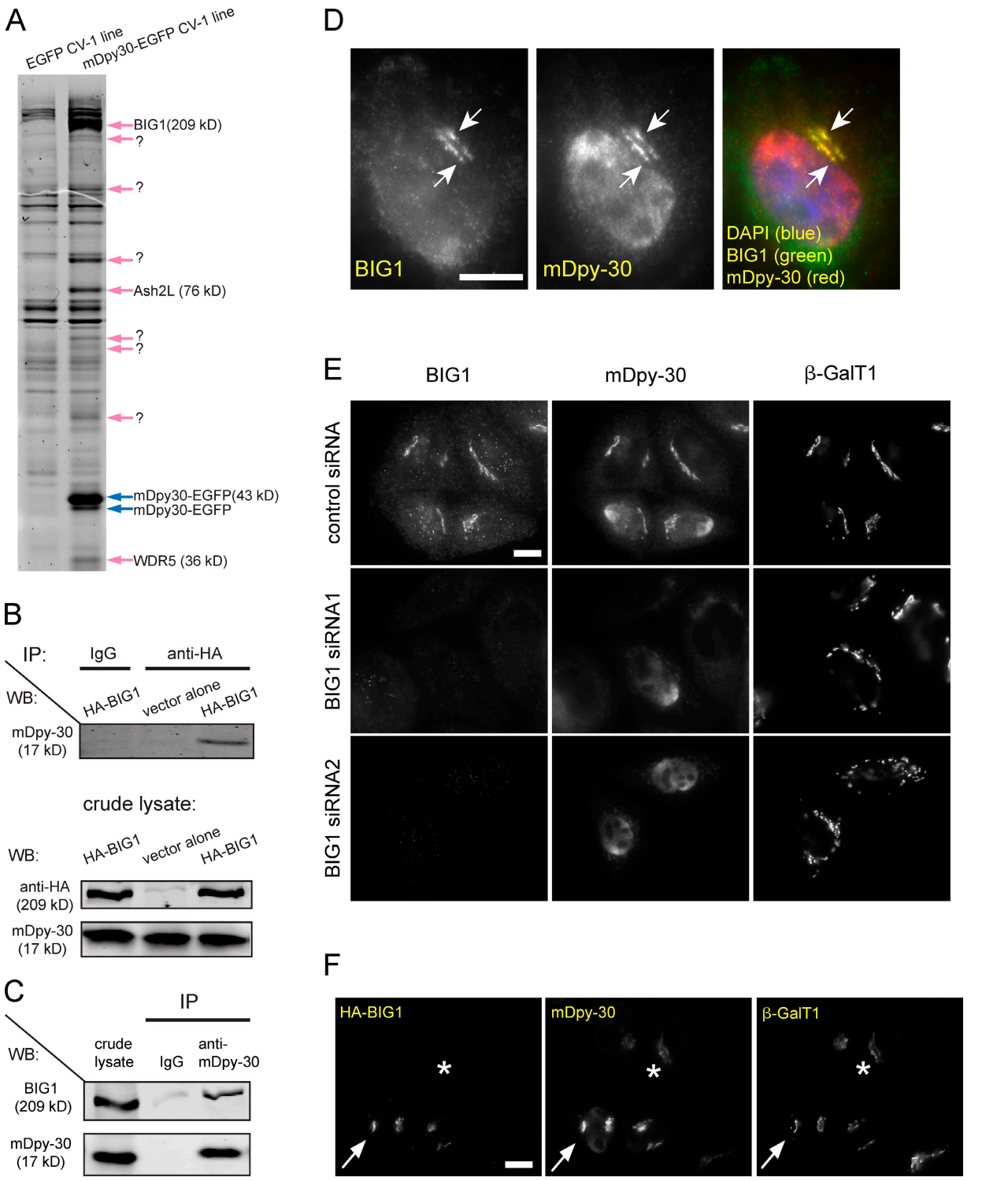

Figure 5. **BIG1-mediated TGN targeting of mDpy-30.** (A) Identification of mDpy-30–interacting proteins by immunopurification and tandem mass spectroscopy from CV-1 cells stably expressing an EGFP fusion of mDpy-30 (see Materials and methods). Question marks indicate bands that remain unidentified. (B and C) Coimmunoprecipitation of endogenous mDpy-30 and transfected HA-tagged BIG1 (B) or endogenous BIG1 (C). An equal amount of cell lysate was used for coimmunoprecipitation in all samples. IP, immunoprecipitation; WB, Western blot. (D) Colocalization of BIG1 and mDpy-30 (indicated by arrows). (E) Influence of depleting BIG1 on the perinuclear targeting of mDpy-30. The punctate staining of BIG1 in the cytoplasm is background. (F) Impact of overexpressing BIG1 on the perinuclear targeting of mDpy-30 (compare asterisks with arrows). Bars, 10 μm.

at the perinuclear TGN region (Fig. 5 D). Interestingly, BIG1 depletion greatly reduced the TGN staining of mDpy-30 without affecting β-GalT1 localization (Fig. 5 E). However, overexpression of BIG1 led to an enhanced staining of perinuclear mDpy-30 (Fig. 5 F). Thus, our data show that BIG1 plays a major role in recruiting mDpy-30 to the TGN.

In this study, we have presented evidence supporting an unexpected link between H3K4MT and endosomal transport. Our findings raise several intriguing questions for future studies. To begin, the mechanism by which mDpy-30 and H3K4MT regulate the endosomal transport remains unknown. One possibility is that mDpy-30, Ash2L, and RbBP5 are components of a yet to be identified methyltransferase complex at the TGN where they affect endosomal transport by controlling the methylation of a trafficking regulator. However, we have not been able to detect the Golgi localization of either Ash2L or RbBP5 using multiple antibodies or their GFP fusions (unpublished data). Another possibility is that the TGN pool of mDpy-30 coordinates with nuclear H3K4MT to modulate endosomal transport. The identification of BIG1 as an mDpy-30–interacting protein may provide clues to the aforementioned question. Both BIG1 and BIG2, a structurally similar ADP ribosylation factor guanine nucleotide exchange factor also found at the TGN (Yamaji et al., 2000), are involved in endosome to TGN transport (Ishizaki et al., 2008) and/or TGN maintenance (Manolea et al., 2008). Intriguingly, the nuclear accumulation of BIG1 in HepG2 cells has been observed under serum starvation conditions (Padilla et al., 2004) and PKA activation (Citterio et al., 2006). It will be interesting to investigate whether mDpy-30 regulates BIG1 function and whether BIG1 influences H3K4MT activity. Another question regards the physiological significance of our observations. Increasing evidence has implicated CIMPR in cell migration (Chapman, 1997; Roshy et al., 2003; Joyce and Hanahan, 2004; Wood and Hulett, 2008). Moreover, Rab4 and -11 (Caswell and Norman, 2006) and VAMP3 (Proux-Gillardeaux et al., 2005; Tayeb et al., 2005) all impact integrin trafficking and cell adhesion/migration. The fact that knockdown of mDpy-30 or other H3K4MT components results in an enrichment of Rab4- or Rab11-positive endosomes at cell protrusions suggests that H3K4MT may regulate cell adhesion/migration via modulating endosomal recycling. It is important to see whether the Rab4- and Rab11-positive compartments accumulated at the protrusions of mDpy-30–depleted cells indeed have a recycling function and to determine what types of cargo proteins besides CIMPR and furin transit via these compartments. Given a key role of local endocytosis and recycling of integrins at the cell leading edge in migration (Caswell and Norman, 2008), it will be tempting to examine how the local trafficking of integrins is changed in cells depleted of mDpy-30 and other H3K4MT components and how this change regulates cell adhesion/migration.

Materials and methods

DNA constructs and reagents

mDpy-30 was cloned from a yeast two-hybrid rat brain cDNA library (Clontech Laboratories, Inc.). The full-length cDNA was PCR amplified and inserted into a bacterial (pUH21.2; a gift from H. Bujard, European Molecular Biology Organization, Heidelberg, Germany) or mammalian (pcDNA3.1; Invitrogen) expression vector. A HA epitope (YPYDVPDYA) or EGFP (Clontech Laboratories, Inc.) was added to the C terminus of mDpy-30 when needed. Rab cDNA clones were gifts from C. Bucci (Università degli Studi di Lecce, Lecce, Italy). The pCMV-HA-BIG1 expression construct was a gift from M. Vaughan (National Institutes of Health, Bethesda, MD). The antibodies used in this study are monoclonal anti-HA (HA.11; Covance), polyclonal anti-HA (ICL), BIG1 (Santa Cruz Biotechnology, Inc.), CD8 (Millipore), p115 (BD), GRASP55 (a gift from F. Barr, University of Liverpool, Liverpool, England, UK), β-GalT1 (a gift from U. Mandel, University of Copenhagen, Copenhagen, Denmark), TGN46 (a gift from S. Ponnambalam, University of Leeds, Leeds, England, UK; Abcam), CIMPR (BioLegend), Lamp1 (Developmental Studies Hybridoma Bank), EEA1 (Sigma-Aldrich), VAMP3 (Synaptic Systems GmbH), and syntaxin 10 (a gift from B.L. Tang and W. Hong, National University of Singapore, Singapore, Republic of Singapore). Biotin-transferrin was obtained from Invitrogen. The siRNAs used in this study are mDpy-30 siRNA1–3 (target sequences: siRNA1, 5′-CACCAAATCCCATTGAATT-3′; siRNA2, 5′-AAACGCAGGTTGCAGAAAA-3′; siRNA3, 5′-AGACAACGTTGAGAGAATA-3′; Thermo Fisher Scientific), Ash2L siRNA1 and -2 (target sequences: siRNA1, 5′-CCGAGTAACTAACTTATTTAA-3′; siRNA2, 5′-CCCGTTTAACAAAGATGGCTA-3′; QIAGEN), RbBP5 siRNA1 and -2 (target sequences: siRNA1, 5′-CAGGTGTCTCTCAACAAGCTA-3′; siRNA2, 5′-ACGGCAGATCGAATAATCAGA-3′; QIAGEN), and SUV39 siRNA1 (target sequence: 5′-GCGGGTCCGTATTGAATGCAA-3′; QIAGEN). The nontargeting control siRNA was obtained from QIAGEN (AllStars Negative Control siRNA).

Expression of recombinant mDpy-30 protein

The cDNA of rat mDpy-30 was cloned into the BamHI–HindIII sites of pUH21.2 vector and transformed into *Escherichia coli*. Transformants were grown in lysogeny broth medium containing 5 g/liter NaCl until the cell density reached an OD_{600} of 0.6. Expression of mDpy-30 protein was then induced using 1 mM isopropyl-β-D-thiogalactopyranoside for 3 h.

Cell culture and transfection

COS-7, CV-1, J774, and HeLa cells were cultured in advanced DME (Invitrogen) supplemented with 4% fetal bovine serum, 2 mM glutamine, and 1× penicillin-streptomycin (Cellgro). The same medium was used to grow flippase recombination enzyme (Flp)–In–CV-1–mDpy-30–HA (Invitrogen) stable cells and HeLa–CD8-CIMPR or HeLa–CD8-furin stable cell lines except that 200 µg/ml hygromycin and 100 µg/ml G418 were added, respectively, for maintenance purposes. To generate Flp-In–CV-1–mDpy-30–HA or Flp-In–CV-1–mDpy-30–EGFP, the mDpy-30–HA or mDpy-30–EGFP fusion was inserted into pcDNA5/Flp recombination target, transfected into Flp-In–CV-1 (Invitrogen) and selected by hygromycin according to the manufacturer's instructions (Invitrogen). When needed, cells were transfected with DNA using FuGENE6 or FuGENE HD (Roche) or siRNA using Lipofectamine 2000 (Invitrogen), and the effects of transfection were investigated 24 h (for DNA) or 48 h (for siRNA) after the transfection, respectively. All siRNAs were used at a concentration of 20 nM.

SDS-PAGE and Western blot analysis

Untreated or transfected cells were solubilized in ice-cold radioimmunoprecipitation assay lysis buffer (50 mM Tris-HCl, pH 8.0, 150 mM NaCl, 1 mM EDTA, 1% NP-40, 0.5% Na deoxycholate, and 0.1% SDS complemented with complete protease inhibitors [Roche] and 1 mM PMSF) and cleared by centrifugation at 4°C. Core histones were prepared using a Histone Preparation Mini kit (Active Motif). Cell lysates were quantitated using the Non-Interfering Protein Assay kit according to the manufacturer's instruction (G-Biosciences) and then denatured in SDS-PAGE loading buffer (with the reducing agent omitted for CIMPR). An equal amount of total protein per sample was then loaded into each well, separated by SDS-PAGE electrophoresis (6–15% gels; Bio-Rad Laboratories), and transferred to Immobilon 0.45-µM polyvinylidene difluoride membranes (Millipore) using a Semi Dry Electroblotting System (Owl). Membranes were incubated with appropriate primary antibody for 1 h in a 1:1 mixture of blocking buffer (Odyssey) and PBS supplemented with 0.1% Tween 20, washed with PBS supplemented with 0.1% Tween 20 (three times for 5 min each), incubated with appropriate secondary antibody (Odyssey) for 30 min in a 1:1 mixture of Odyssey blocking buffer and PBS supplemented with 0.1% Tween 20 and 0.01% SDS, washed first with PBS supplemented with 0.1% Tween 20 (three times for 5 min each) followed with PBS for 5 min, and dried in the dark. Fluorescence quantification was performed on an Infrared Imaging System (model 9120; Odyssey).

Immunofluorescence analysis

Cells or transfected cells were fixed in PBS containing 3% formaldehyde for 15 min, permeabilized with PBS containing 0.1% saponin or Triton X-100 for 15 min, blocked in Blocker Casein in PBS (Thermo Fisher Scientific) containing 5% goat serum for 30 min, incubated with primary antibody in the blocking buffer for 2 h, washed in PBS three times for 5 min each, incubated with fluorophore-conjugated secondary antibody in the blocking buffer for 1 h, washed in PBS three times for 5 min each, incubated in PBS containing 1 µg/ml DAPI for 5 min, and washed in PBS three times for

5 min each. Immunostained cells were allowed to air dry, mounted, and examined with a microscope (IX-81; Olympus).

Conventional microscopy

An IX-81 microscope was used in the epifluorescence experiments. A Plan-Apochromat 60× oil total internal reflection fluorescence microscope objective (Olympus) with a 1.45 aperture was used throughout. All microscopy was performed at room temperature. Slides were mounted in SlowFade Gold antifade reagent (Invitrogen). Our secondary antibodies were conjugated to either Alexa Fluor 488 or Rhodamine red-X (appearing as green and red in the images, respectively). A monochrome digital camera (Evolution QEi; Media Cybernetics) mounted to the Olympus microscope and the in vivo acquisition software version 3.2.0 (Media Cybernetics) were used to capture images and analyze the microscope images. Finally, to crop the images for publication, we used Photoshop (Adobe) and Illustrator (Adobe) software packages.

Confocal microscopy

Images of the cells were captured with a laser-scanning confocal microscope (Fluoview 500; Olympus) with a 40× Plan-Apochromat NA 1.3 lens. Two laser lines were used at 488 and 543 nm to excite the fluorochromes. Sequential color image capture was used to collect images. To record the distribution of label from apical to basal portions of the cell, a z series of 20 images was captured of the cells at 0.5-µm steps.

Immunoprecipitation

Cells or transfected cells were solubilized in ice-cold NP-40 lysis buffer (50 mM Tris-HCl, pH 8.0, 150 mM NaCl, 1 mM EDTA, and 1% NP-40 complemented with complete protease inhibitor and 1 mM PMSF) and cleared by centrifugation at 4°C. Immunoprecipitates were collected by a brief centrifugation after incubating the supernatant with a primary antibody for 1 h followed by protein G–Sepharose (Invitrogen) for 2 h at 4°C. The Sepharose beads were washed four times in ice-cold lysis buffer and once with PBS, and the bound proteins were eluted with SDS–PAGE sample buffer at 55°C for 1 h or at 90°C for 10 min.

Identification of mDpy-30–interacting proteins by immunopurification and mass spectroscopy

To purify mDpy-30–associated proteins, a mouse monoclonal anti-GFP antibody covalently linked to magnetic microbeads (µMACS GFP Tagged Protein Isolation kit; Miltenyi Biotec) was used to immunoprecipitate the mDpy-30–EGFP and its associated proteins from the Flp-In–CV-1–mDpy-30–EGFP stable cells under a stringent wash condition (650 mM NaCl, 1% Igepal CA-630, 0.5% Na deoxycholate, 0.1% SDS, and 50 mM Tris-HCl, pH 8.0). Flp-In–CV-1 cells stably expressing EGFP alone were included as a negative control. The immunoprecipitates were then separated on SDS-PAGE and stained with SYPRO RUBY. The putative mDpy-30–associated protein bands were excised, eluted, and subjected to digestion, and the resulting peptides were resolved on a reverse-phase liquid chromatography system and detected by coupled tandem mass spectrometry (microcapillary high performance liquid chromatography system [NanoFlow 1100; Agilent Technologies] connected to a mass spectrometer [ESI-QToF 2; Micromass]).

Internalization assay

HeLa–CD8-CIMPR (or HeLa–CD8-furin) cells were blocked in PBS containing 2% normal goat serum for 30 min and incubated with 1 µg/ml anti-CD8 antibody in PBS containing 2% goat serum for 1 h at 0°C to label the surface fusion proteins. After removing the unbound antibodies by PBS wash at 0°C three times for 5 min each, cells were transferred into prewarmed culture medium and returned to 37°C to allow internalization to proceed for the indicated periods of time before immunofluorescence study. To monitor the endosomal transport of endogenous CIMPR in HeLa cells, anti-CIMPR antibody was added to the culture medium at 5 µg/ml for 1 h at 37°C before fixation to enhance the internalization signal by allowing continuous labeling and internalization.

Online supplemental material

Fig. S1 shows the characterization of the rabbit polyclonal anti–mDpy-30 antibody using Western blot analyses, immunoprecipitation, and immunofluorescence microscopy. Fig. S2 shows the characterization of three different mDpy-30 siRNAs and the knockdown efficiency of different pools of mDpy-30 as well as the effect of mDpy-30 knockdown on H3K4 trimethylation. Online supplemental material is available at http://www.jcb.org/cgi/content/full/jcb.200902146/DC1.

We are grateful to the following individuals for their gifts: Drs. C. Bucci for the Rab cDNA clones, M. Vaughan for the pCMV-HA-BIG1 expression construct, F. Barr for anti-GRASP55, S. Ponnambalam for anti-TGN46, U. Mandel for anti–β-GalT1, W. Hong for anti–syntaxin 10, and C. Jackson (National Institutes of Health, Bethesda, MD) for anti-BIG1 antibodies.

This work was supported in part by a research grant from the Cancer Research Coordinating Committee.

Submitted: 27 February 2009
Accepted: 9 July 2009

References

Cai, H., K. Reinisch, and S. Ferro-Novick. 2007. Coats, tethers, Rabs, and SNAREs work together to mediate the intracellular destination of a transport vesicle. *Dev. Cell*. 12:671–682.

Caswell, P.T., and J.C. Norman. 2006. Integrin trafficking and the control of cell migration. *Traffic*. 7:14–21.

Caswell, P., and J. Norman. 2008. Endocytic transport of integrins during cell migration and invasion. *Trends Cell Biol.* 18:257–263.

Chapman, H.A. 1997. Plasminogen activators, integrins, and the coordinated regulation of cell adhesion and migration. *Curr. Opin. Cell Biol.* 9:714–724.

Chen, J.W., T.L. Murphy, M.C. Willingham, I. Pastan, and J.T. August. 1985. Identification of two lysosomal membrane glycoproteins. *J. Cell Biol.* 101:85–95.

Cho, Y.W., T. Hong, S. Hong, H. Guo, H. Yu, D. Kim, T. Guszczynski, G.R. Dressler, T.D. Copeland, M. Kalkum, and K. Ge. 2007. PTIP associates with MLL3- and MLL4-containing histone H3 lysine 4 methyltransferase complex. *J. Biol. Chem.* 282:20395–20406.

Citterio, C., H.D. Jones, G. Pacheco-Rodriguez, A. Islam, J. Moss, and M. Vaughan. 2006. Effect of protein kinase A on accumulation of brefeldin A-inhibited guanine nucleotide-exchange protein 1 (BIG1) in HepG2 cell nuclei. *Proc. Natl. Acad. Sci. USA*. 103:2683–2688.

Cocucci, E., G. Racchetti, M. Rupnik, and J. Meldolesi. 2008. The regulated exocytosis of enlargeosomes is mediated by a SNARE machinery that includes VAMP4. *J. Cell Sci.* 121:2983–2991.

Dou, Y., T.A. Milne, A.J. Ruthenburg, S. Lee, J.W. Lee, G.L. Verdine, C.D. Allis, and R.G. Roeder. 2006. Regulation of MLL1 H3K4 methyltransferase activity by its core components. *Nat. Struct. Mol. Biol.* 13:713–719.

Ganley, I.G., E. Espinosa, and S.R. Pfeffer. 2008. A syntaxin 10–SNARE complex distinguishes two distinct transport routes from endosomes to the trans-Golgi in human cells. *J. Cell Biol.* 180:159–172.

Ghosh, P., N.M. Dahms, and S. Kornfeld. 2003. Mannose 6-phosphate receptors: new twists in the tale. *Nat. Rev. Mol. Cell Biol.* 4:202–212.

Ghosh, R.N., W.G. Mallet, T.T. Soe, T.E. McGraw, and F.R. Maxfield. 1998. An endocytosed TGN38 chimeric protein is delivered to the TGN after trafficking through the endocytic recycling compartment in CHO cells. *J. Cell Biol.* 142:923–936.

Hsu, D.R., P.T. Chuang, and B.J. Meyer. 1995. DPY-30, a nuclear protein essential early in embryogenesis for *Caenorhabditis elegans* dosage compensation. *Development*. 121:3323–3334.

Huang, J., and S.L. Berger. 2008. The emerging field of dynamic lysine methylation of non-histone proteins. *Curr. Opin. Genet. Dev.* 18:152–158.

Hughes, C.M., O. Rozenblatt-Rosen, T.A. Milne, T.D. Copeland, S.S. Levine, J.C. Lee, D.N. Hayes, K.S. Shanmugam, A. Bhattacharjee, C.A. Biondi, et al. 2004. Menin associates with a trithorax family histone methyltransferase complex and with the hoxc8 locus. *Mol. Cell*. 13:587–597.

Ishizaki, R., H.W. Shin, H. Mitsuhashi, and K. Nakayama. 2008. Redundant roles of BIG2 and BIG1, guanine-nucleotide exchange factors for ADP-ribosylation factors in membrane traffic between the trans-Golgi network and endosomes. *Mol. Biol. Cell*. 19:2650–2660.

Joyce, J.A., and D. Hanahan. 2004. Multiple roles for cysteine cathepsins in cancer. *Cell Cycle*. 3:1516–1519.

Kanwar, N., A. Fayyazi, B. Backofen, M. Nitsche, R. Dressel, and G.F. von Mollard. 2008. Thymic alterations in mice deficient for the SNARE protein VAMP8/endobrevin. *Cell Tissue Res.* 334:227–242.

Mallard, F., B.L. Tang, T. Galli, D. Tenza, A. Saint-Pol, X. Yue, C. Antony, W. Hong, B. Goud, and L. Johannes. 2002. Early/recycling endosomes-to-TGN transport involves two SNARE complexes and a Rab6 isoform. *J. Cell Biol.* 156:653–664.

Manolea, F., A. Claude, J. Chun, J. Rosas, and P. Melancon. 2008. Distinct functions for Arf guanine nucleotide exchange factors at the Golgi complex: GBF1 and BIGs are required for assembly and maintenance of the Golgi stack and trans-Golgi network, respectively. *Mol. Biol. Cell*. 19:523–535.

Markgraf, D.F., K. Peplowska, and C. Ungermann. 2007. Rab cascades and tethering factors in the endomembrane system. *FEBS Lett.* 581:2125–2130.

Maxfield, F.R., and T.E. McGraw. 2004. Endocytic recycling. *Nat. Rev. Mol. Cell Biol.* 5:121–132.

Meresse, S., J.P. Gorvel, and P. Chavrier. 1995. The rab7 GTPase resides on a vesicular compartment connected to lysosomes. *J. Cell Sci.* 108:3349–3358.

Miller, T., N.J. Krogan, J. Dover, H. Erdjument-Bromage, P. Tempst, M. Johnston, J.F. Greenblatt, and A. Shilatifard. 2001. COMPASS: a complex of proteins associated with a trithorax-related SET domain protein. *Proc. Natl. Acad. Sci. USA*. 98:12902–12907.

Morinaga, N., J. Moss, and M. Vaughan. 1997. Cloning and expression of a cDNA encoding a bovine brain brefeldin A-sensitive guanine nucleotide-exchange protein for ADP-ribosylation factor. *Proc. Natl. Acad. Sci. USA*. 94:12926–12931.

Nelson, D.S., C. Alvarez, Y.S. Gao, R. Garcia-Mata, E. Fialkowski, and E. Sztul. 1998. The membrane transport factor TAP/p115 cycles between the Golgi and earlier secretory compartments and contains distinct domains required for its localization and function. *J. Cell Biol.* 143:319–331.

Ng, S.S., W.W. Yue, U. Oppermann, and R.J. Klose. 2009. Dynamic protein methylation in chromatin biology. *Cell. Mol. Life Sci.* 66:407–422.

Nielsen, E., A.Y. Cheung, and T. Ueda. 2008. The regulatory RAB and ARF GTPases for vesicular trafficking. *Plant Physiol.* 147:1516–1526.

Padilla, P.I., G. Pacheco-Rodriguez, J. Moss, and M. Vaughan. 2004. Nuclear localization and molecular partners of BIG1, a brefeldin A-inhibited guanine nucleotide-exchange protein for ADP-ribosylation factors. *Proc. Natl. Acad. Sci. USA*. 101:2752–2757.

Ponnambalam, S., M. Girotti, M.L. Yaspo, C.E. Owen, A.C. Perry, T. Suganuma, T. Nilsson, M. Fried, G. Banting, and G. Warren. 1996. Primate homologues of rat TGN38: primary structure, expression and functional implications. *J. Cell Sci.* 109:675–685.

Proux-Gillardeaux, V., J. Gavard, T. Irinopoulou, R.M. Mege, and T. Galli. 2005. Tetanus neurotoxin-mediated cleavage of cellubrevin impairs epithelial cell migration and integrin-dependent cell adhesion. *Proc. Natl. Acad. Sci. USA*. 102:6362–6367.

Rea, S., F. Eisenhaber, D. O'Carroll, B.D. Strahl, Z.W. Sun, M. Schmid, S. Opravil, K. Mechtler, C.P. Ponting, C.D. Allis, and T. Jenuwein. 2000. Regulation of chromatin structure by site-specific histone H3 methyltransferases. *Nature*. 406:593–599.

Roguev, A., D. Schaft, A. Shevchenko, W.W. Pijnappel, M. Wilm, R. Aasland, and A.F. Stewart. 2001. The *Saccharomyces cerevisiae* Set1 complex includes an Ash2 homologue and methylates histone 3 lysine 4. *EMBO J.* 20:7137–7148.

Roshy, S., B.F. Sloane, and K. Moin. 2003. Pericellular cathepsin B and malignant progression. *Cancer Metastasis Rev.* 22:271–286.

Ruthenburg, A.J., C.D. Allis, and J. Wysocka. 2007. Methylation of lysine 4 on histone H3: intricacy of writing and reading a single epigenetic mark. *Mol. Cell*. 25:15–30.

Schneider, J., A. Wood, J.S. Lee, R. Schuster, J. Dueker, C. Maguire, S.K. Swanson, L. Florens, M.P. Washburn, and A. Shilatifard. 2005. Molecular regulation of histone H3 trimethylation by COMPASS and the regulation of gene expression. *Mol. Cell*. 19:849–856.

Seaman, M.N. 2004. Cargo-selective endosomal sorting for retrieval to the Golgi requires retromer. *J. Cell Biol.* 165:111–122.

Shilatifard, A. 2008. Molecular implementation and physiological roles for histone H3 lysine 4 (H3K4) methylation. *Curr. Opin. Cell Biol.* 20:341–348.

Shorter, J., R. Watson, M.E. Giannakou, M. Clarke, G. Warren, and F.A. Barr. 1999. GRASP55, a second mammalian GRASP protein involved in the stacking of Golgi cisternae in a cell-free system. *EMBO J.* 18:4949–4960.

Steward, M.M., J.S. Lee, A. O'Donovan, M. Wyatt, B.E. Bernstein, and A. Shilatifard. 2006. Molecular regulation of H3K4 trimethylation by ASH2L, a shared subunit of MLL complexes. *Nat. Struct. Mol. Biol.* 13:852–854.

Su, I.H., M.W. Dobenecker, E. Dickinson, M. Oser, A. Basavaraj, R. Marqueron, A. Viale, D. Reinberg, C. Wulfing, and A. Tarakhovsky. 2005. Polycomb group protein ezh2 controls actin polymerization and cell signaling. *Cell*. 121:425–436.

Tayeb, M.A., M. Skalski, M.C. Cha, M.J. Kean, M. Scaife, and M.G. Coppolino. 2005. Inhibition of SNARE-mediated membrane traffic impairs cell migration. *Exp. Cell Res.* 305:63–73.

Ullrich, O., S. Reinsch, S. Urbe, M. Zerial, and R.G. Parton. 1996. Rab11 regulates recycling through the pericentriolar recycling endosome. *J. Cell Biol.* 135:913–924.

Wood, R.J., and M.D. Hulett. 2008. Cell surface-expressed cation-independent mannose 6-phosphate receptor (CD222) binds enzymatically active heparanase independently of mannose 6-phosphate to promote extracellular matrix degradation. *J. Biol. Chem.* 283:4165–4176.

Wu, C.C., M.J. MacCoss, G. Mardones, C. Finnigan, S. Mogelsvang, J.R. Yates III, and K.E. Howell. 2004. Organellar proteomics reveals Golgi arginine dimethylation. *Mol. Biol. Cell*. 15:2907–2919.

Yamaji, R., R. Adamik, K. Takeda, A. Togawa, G. Pacheco-Rodriguez, V.J. Ferrans, J. Moss, and M. Vaughan. 2000. Identification and localization of two brefeldin A-inhibited guanine nucleotide-exchange proteins for ADP-ribosylation factors in a macromolecular complex. *Proc. Natl. Acad. Sci. USA*. 97:2567–2572.